Initial Results for Hybrid SPECT–Conjugate-View Tumor Dosimetry in ^{131}I-Anti-B_1 Antibody Therapy of Previously Untreated Patients with Lymphoma

Kenneth F. Koral, Yuni Dewaraja, Jia Li, Carla L. Barrett, Denise D. Regan, Kenneth R. Zasadny, Stephen G. Rommelfanger, Issac R. Francis, Mark S. Kaminski, and Richard L. Wahl

Department of Internal Medicine, Divisions of Nuclear Medicine and Hematology/Oncology, and Department of Radiology, University of Michigan Medical Center, Ann Arbor, Michigan

A study of the use of ^{131}I-labeled anti-B_1 monoclonal antibody, proceeded by an unlabeled predose, for therapy of previously untreated non-Hodgkin's lymphoma patients has recently been completed at the University of Michigan, Ann Arbor. More than half of the patients treated were imaged intratherapy with SPECT to separate apparently large tumors, unresolved by conjugate views, into individual ones specified by CT scan. The dosimetry of these tumors is reported here. **Methods:** The activity-quantification procedure used 3-dimensional CT-to-SPECT fusion so that attenuation maps could be computed from CT and that volumes of interest could be drawn on the CT slices and transferred to the SPECT images. Daily conjugate-view images after a tracer dose of labeled anti-B_1 antibody followed by an unlabeled predose provided the shape of the time–activity curve for the calculation of therapy dosimetry. Reconstructed SPECT counts that were within a volume of interest were converted to activity by using a background-and-radius-adaptive conversion factor. Activities were increased for tumors less than 200 g using a recovery-coefficient factor derived from activity measurements for a set of spheres with volumes ranging from 1.6 to 200 cm^3. The calculated tumor radiation absorbed dose was based, in part, on the CT volume and on the intratherapy–SPECT activity. **Results:** The mean of the radiation dose values for 131 abdominal or pelvic tumors in 31 patients was 616 cGy with a standard deviation of ±50 cGy. The largest dose was 40 Gy and the smallest dose was 73 cGy. The mean volume for the tumors was 59.2 ± 11.2 cm^3. The correlation coefficient between absorbed dose and tumor volume was small ($r^2 = 0.007$), and the slope of the least-squares fit represented a decrease of only 36.4 cGy per 100 cm^3 increase in volume. This small slope may reflect a characteristic of anti-B_1 antibody therapy that is important for its success. The mean absorbed dose per unit administered activity was 1.83 ± 0.145 Gy/GBq. The largest value was 12.6 Gy/GBq, and the smallest value was 0.149 Gy/GBq. The mean dose for 9 axillary tumors in 5 patients was significantly lower than the average dose for abdominal and pelvic tumors ($P = 0.01$). Therefore, axillary tumors should be grouped separately in assessing dose–response relationships. Anecdotal patient results tended to verify the validity of using the shape of the conjugate-view time–activity curve for the average SPECT–intratherapy curve. However, there was also an indication that the shape varies somewhat for individual tumors with respect to time to peak. **Conclusion:** Hybrid SPECT–conjugate-view dosimetry provided radiation absorbed dose estimates for the individual patient tumors that were resolved by CT.

Key Words: tumor dosimetry; ^{131}I; radioimmunotherapy; lymphoma; SPECT; fusion

J Nucl Med 2000; 41:1579–1586

Radioimmunotherapy (RIT) with ^{131}I-labeled monoclonal antibodies is showing great promise in the treatment of follicular-lymphoma cancer, also known as non-Hodgkin's lymphoma (*1*–*6*). At the University of Michigan, a phase 2 ^{131}I-labeled-anti-B_1 monoclonal antibody therapy study of previously untreated patients has been completed and preliminary response rates have been reported (*6*). However, clinical correlates to the degree of response have not been easy to find. One multivariate analysis that included patients from 6 clinical trials (phase 1, 2, or 3) had some success; however, tumor radiation absorbed dose as evaluated by conjugate views was not tested as an explanatory variable (*7*). The study of tumor radiation absorbed dose in previously untreated anti-B_1 antibody patients, for which results are reported here, has been undertaken in hopes of ultimately finding a correlation between tumor radiation absorbed dose and response.

In dosimetry for RIT studies, it is common practice (*1*,*8*,*9*) to assume that the therapy time–activity curve is equal to the tracer time–activity curve after scaling the ordinate (i.e., the activity axis) by the ratio of administered activities. This assumption is equivalent to the assumption that the ratio of therapy percentage infused dose over tracer percentage infused dose equals 1. Both in the past (*10*) and in this article, results from daily conjugate-view images that are acquired after the administration of a tracer amount of

Received Oct. 12, 1999; revision accepted Feb. 16, 2000.

For correspondence or reprints contact: Kenneth F. Koral, PhD, University of Michigan, Division of Nuclear Medicine, B1G412 UH, Ann Arbor, MI 48109-0028.

labeled anti-B_1 antibody have been used in the dosimetry calculation. However, only the assumption that the time–activity curve for a tumor seen on conjugate views after a tracer administration gives the shape of the time–activity curve for that tumor after the therapy administration is made. The scale of the ordinate of that curve is allowed to be different from what one would obtain by the scaling assumption and has been assessed with an intratherapy SPECT scan.

Recently, in a small subset of patients previously untreated with anti-B_1 antibody, good statistical support for the hypothesis that the population average of the ratio of therapy percentage infused dose (%ID) over tracer %ID is 1 has been reported (*11*). However, the range of the ratio was 0.71–1.82 for tumors evaluated by SPECT during both tracer and therapy and was 0.70–1.35 for tumors evaluated by conjugate views during both tracer and therapy. Because the ranges were fairly large with both methods, 1 interpretation is that accuracy greater than that achieved with the scaling assumption is obtained by allowing the therapy/tracer tumor activity ratio to be different than 1.

An explicit feature of this study is obtaining separate dosimetric results for tumors that are resolvable by CT even if they are not resolvable by conjugate views. This refinement is made possible by the fusion of the patient CT scan to the intratherapy–SPECT scan. Through this fusion, the tumor boundaries are chosen on the CT scan and then applied to the SPECT scan. Thus, an individual SPECT activity estimate is obtained for each tumor, defined by a combination of CT regions of interest. In the current implementation, the shape from a single time–activity curve, obtained by tracer conjugate views, is usually applied to the dosimetric analysis for the multiple individual tumors that make up the single conjugate-view tumor.

TABLE 1
Patient Demographics

Patient no.	Age (y)	Sex	Location of evaluated tumors
1	30	M	Abdomen
2	52	M	Abdomen
3	38	M	Pelvis
5	38	F	Abdomen
7	56	M	Abdomen/pelvis
10	28	F	Abdomen
11	36	M	Abdomen
13	55	F	Abdomen
14	46	F	Abdomen
15	67	M	Abdomen
16	32	F	Abdomen
24	44	M	Abdomen
27	64	F	Abdomen
30	43	F	Abdomen
31	44	F	Abdomen
32	50	M	Abdomen
34	41	M	Abdomen
36	51	F	Abdomen
37	36	F	Abdomen
39	40	M	Abdomen
42	52	M	Abdomen
43	55	M	Abdomen
44	23	F	Pelvis
46	55	F	Pelvis
51	51	M	Axilla
55	42	M	Abdomen/axilla
56	48	F	Pelvis
59	59	F	Pelvis
60	55	F	Pelvis
61	41	M	Axilla
67	49	M	Abdomen/axilla
69	47	F	Abdomen/pelvis
71	30	F	Pelvis/axilla

MATERIALS AND METHODS

Patients

Thirty-three previously untreated patients (average age, 45.4 y; range, 23–67 y) had either their chest, abdomen, or pelvis imaged by SPECT after the therapy administration of combined anti-B_1 and were analyzed by hybrid SPECT–conjugate-view tumor dosimetry. Patients' data are given in Table 1. When axilla is listed with abdomen or pelvis as the imaging site, the patient had 2 separate scans.

Administered Activity

Patients underwent evaluative conjugate-view imaging with a tracer dose of ^{131}I-labeled anti-B_1 antibody as part of anti-B_1 antibody therapy protocol for which they gave informed consent. It was the first time the patients were being treated with anti-B_1 antibody in all cases. For the 1-wk tracer evaluation, patients were given a 450-mg predose of unlabeled anti-B_1 antibody infused over 1 h and then an infusion of anti-B_1 antibody labeled with about 185 MBq (5 mCi) ^{131}I. This evaluation was then followed by the administration of a therapy dose on day 7. This dose consisted of an infusion of the same amount of predose as used in the evaluation, followed by the administration of a higher activity of labeled anti-B_1 antibody that had been calculated to give a 65–75 cGy total-body radiation absorbed dose. The usual time for intratherapy–SPECT imaging was from 2 to 3 d after the therapy administration. Patients gave their separate written informed consent for all SPECT imaging.

Hybrid SPECT–Conjugate-View Dosimetry

Image Acquisition. For conjugate-view acquisition, a Siemens (Hoffman Estates, IL) dual-head, whole-body imager was used. Images were recorded daily starting from 1 to 2 h after the tracer administration. A 20% energy window was automatically set on the 364-keV photopeak of ^{131}I. Whole-body, simultaneously acquired anterior and posterior views were acquired in 400 s. ''Spot views'' of tumor-involved regions were similarly acquired using 15 min per view. In addition, on 1 d of the 7-d imaging series, a 10-min transmission scan was obtained for each spot-view region by placing a ^{57}Co flood source on the bottom head of the camera and recording the data from the top head.

For both SPECT and CT acquisition, patients were placed with their arms above their heads on the usual imaging tables. With about half of the patients, ink-mark crosses were made on the skin at 5 locations within the field of view of the SPECT scan. Before CT, small lead markers were placed at the center of these ink marks, and before SPECT, 6-mm filter paper disks soaked in ^{131}I solution and sealed with tape were placed over the same locations. Each disk contained about 0.926 MBq (25 μCi) of radioactivity. For

tracer SPECT acquisitions, the activity level was only about one fifth as much.

For SPECT acquisitions, 2 different models of a triple-head Picker Prism (Cleveland, OH) camera, a 20-min acquisition, and 60 angles over 360° were used. A circular orbit was used in all cases. For an abdominal scan and 1 camera head, a typical projection contained 224,176 counts in the main window, which implies approximately 13.5 million counts for the acquisition. A 64 × 64 projection-image matrix size was used. The protocol for each model was slightly different as described below. For patients with identification numbers less than 16 (10 patients), a model 3000 XP was used, and for patients with identification number greater than 16 (22 patients), a model 3000 was used. The patient with identification number equal to 16 was scanned with a method that mixed the features of the 2 protocols. For each head of the 3000 XP model, the photopeak window was set at a width of 20% and was visually centered on the ^{131}I photopeak. For each head of the model 3000, 3 energy windows were used: a 20% photopeak window and two 6% windows, 1 immediately below and the other immediately above the photopeak window. The 20% window was again visually centered on the ^{131}I photopeak.

Conjugate-View Analysis. The geometric mean of net anterior and posterior whole-body counts was calculated at each of the multiple imaging time points. Percent injected activity in the total body was obtained for each time point by assuming that the total counts for the earliest time point corresponded to the entire activity of the tracer injection. (The image for the first time point was acquired prevoiding.) For activity quantification of tumors, regions of interest (ROIs) were drawn on corresponding regions on the anterior and posterior projections that composed the ''spot view'' and the tumor counts were obtained. An estimate of the count contribution from tissue in front of and behind the tumor was then made using a 2-step procedure. First, an ROI was drawn in an extratumor region that was near the tumor ROI and for which the body thickness was the same. Counts were obtained and scaled for any difference in size between the tumor ROI and extratumor ROI. Second, from the CT scan, an estimate was made of the fraction of the body thickness in the anterior–posterior direction that was occupied by nontumor tissue. The counts obtained previously from the extratumor ROI were decreased, by multiplying by this fraction, and then were subtracted from the tumor count. The geometric mean of anterior and posterior counts was then obtained and converted to activity. The calibration procedure to allow the conversion has been discussed in a previous publication (*12*).

The collective tumor mass for the tumor being quantified was determined from the areas of the ROI of all tumors that were in a line of projection with the activity hot spot. Because tumors that can be spatially separated on the CT scan were often included in a single conjugate-view evaluation, the tumor evaluated by conjugate views was called a composite tumor and the tumor evaluated from the CT scan was called an individual tumor. Each CT ROI had to overlap another ROI from 1 slice to the next or had to be contiguous in a single slice to be combined to form an individual tumor.

Deadtime Correction. Before SPECT reconstruction, the projection data from each head were corrected for camera deadtime. A paralyzable model was assumed, and deadtime constants were determined according to a method previously described (*13*). Separate deadtime constants were used for each head. Data were corrected projection by projection. For the model 3000 camera, the deadtime correction factor was determined from the counting rate corresponding to the sum of the rates from the 3 windows. The single correction factor was then applied to the data in each of the 3 windows.

Reconstruction Using CT–SPECT Fusion. Our reconstruction procedure used 3-dimensional CT–SPECT fusion. This fusion provided the attenuation map for attenuation correction during reconstruction by converting CT voxel values in Hounsfield units to the ^{131}I attenuation coefficients. In addition, the fusion allowed us to draw tumor ROIs and total-body ROIs on digital CT scans and then appropriately apply these ROIs to the reconstructed SPECT image sets.

The method for the use of CT–SPECT fusion is the low-noise-data method derived by Koral et al. (*11*). Needed extra details are as follows: (a) it was unnecessary to handle the data from each head in a completely independent way because the reconstructed images exhibited very good co-registration. (b) When markers had been placed on the skin at the same location in both modalities, the fusion relied on their relative location in the filtered-backprojection image set and in the CT scan set; otherwise, fusion depended on an image-brightness, mutual-information (''MIAMI Fuse'') algorithm (*14*). (c) For the model 3000 XP camera, data were reconstructed without an explicit compensation for patient scatter (patient scatter was handled implicitly in the quantification procedure). For the model 3000 camera, a pixel-by-pixel estimate of the patient-scatter counting rate was determined for each projection using the triple-energy window (TEW) method (*15*). These estimates were then input into the space-alternating generalized expectation-maximization (SAGE) iterative algorithm (*16*), which reconstructed activity while compensating for the scatter.

^{131}I Quantification. To produce an estimate of tumor activity, the values for reconstructed counts were converted to activity by using a conversion factor that was sensitive to the measured extratumor activity (alias background) and to the known radius of rotation of the camera orbit. A different conversion factor was calculated for each camera head and separately applied to the appropriate estimate of reconstructed counts. For the model 3000 XP camera, the description of the procedure for the calibration of the conversion factor and of the validation of the method is found in (*17*). For the model 3000 camera, similar information is found in (*18*).

Final activity estimates for individual tumors were corrected (increased) for tumors <200 mL by applying a recovery coefficient that depended on individual tumor volume (V). The description of the procedure for measuring the recovery coefficients and the resultant curves for recovery-coefficient correction factor versus volume are found in (*19*). Three final SPECT values for tumor activity were determined, 1 from each of the 3 heads.

Tumor Dosimetry. The first step in the dosimetry was to calculate the radiation absorbed dose to the composite tumor during therapy on the basis of tracer conjugate views and on the scaling assumption. MIRD methods were used (*20*); the total dose included contributions from activity in the tumor itself (the self-dose) and contributions from the activity in the remainder of the body. To calculate the self-dose, the individual data points for tumor activity as a function of time were divided by the tracer-administered activity to yield %ID. These values were fit by a triexponential expression. The integral under this curve gave the tumor residence time. The component of the self-dose from nonpenetrating radiation was calculated from this residence time, the volume estimate for the composite tumor, and appropriate constants. The other component of the self-dose, that from penetrating radiation originating from within the tumor, was

calculated from these parameters plus the known absorbed fraction for a sphere of the same volume as the composite tumor. To perform the calculation of the dose from the penetrating radiation caused by the activity in the remainder of the body, the whole-body clearance curve was fit by a monoexponential expression. The integral under this curve divided by the administered activity gave the whole-body residence time. Then the tumor residence time was subtracted from the whole-body residence time to yield the residence time for the activity in the remainder of the body. From this value and the remainder-of-body S factor, the penetrating-radiation component of the dose was determined. The total tracer absorbed dose was the sum of the self-dose and the remainder-of-body dose. The total therapy radiation absorbed dose was calculated by scaling this tracer dose by the ratio of infused activities.

For hybrid SPECT–conjugate-view dosimetry, the shape of the intratherapy time–%ID curve was taken from the triexponential fit to the tracer time–%ID curve for the composite tumor that was spatially closest. However, values along the %ID axis were reduced by multiplication by the ratio of the individual tumor volume over the composite tumor volume. This multiplication produces a time–%ID curve for part of the composite tumor. The tracer absorbed dose for this part of the composite tumor is the same as the tracer absorbed dose for the entire composite tumor. (%ID has been reduced but so has volume, by the same factor, so radiation dose, the division of the 2, remains the same.) Next, the intratherapy–SPECT activity for the individual tumor at a specific time after administration was converted to a SPECT–%ID value by dividing by the therapy-administered activity. Then, conjugate-view values along the tracer %ID axis for part of the composite tumor were further modified by requiring the time–%ID curve for part of the composite tumor to pass through the SPECT-measured value for %ID. The normalization constant is that factor that has to be applied to the ordinate of the curve such that it passes through the SPECT value. This normalization constant represents the dosimetric effect from including an intratherapy SPECT measurement in place of using solely tracer conjugate-view measurements plus the scaling assumption. Once the normalization factor was thus determined, the hybrid SPECT–conjugate-view estimate of the radiation absorbed dose for the individual tumor was calculated as the product of this normalization factor multiplied by the value for the total therapy radiation absorbed dose for the composite tumor.

Three values for the radiation absorbed dose were determined, 1 from each of the 3 heads. The mean of these 3 values is reported as the final radiation absorbed dose value, D. We note that the SEM divided by the mean was usually around 2%–3% but increased to around 10% for the smallest tumors.

Tests of Assumption About Time–Activity Curve Shape

Intratherapy SPECT Time Series. Only patient 16 was scanned 3 times with SPECT after administration of the therapy infusion. The time period covered was 55 h. The first scan was at 3.73 d after infusion, about 2 d later than our usual time for intratherapy SPECT. This scan sequence provides a means to check the rate of activity washout, as assessed by intratherapy SPECT, against that provided by intraevaluation conjugate views. Recall that, under our assumptions, the washout rate of the time–activity curve from intraevaluation conjugate views, as well as the rest of the shape, is used for intratherapy SPECT to help compute the dosimetry for each individual SPECT tumor.

This particular patient was scanned with the 3000 XP camera but TEW scatter compensation was applied. Appropriate deadtime correction factors and an appropriate calibration were available for the parameters and so were applied to the multiple scans of this 1 patient.

Intraevaluation SPECT Time Series. Patient 43 was scanned with SPECT 6 times after the anti-B_1–antibody tracer infusion was administered for evaluation purposes. Conjugate-view scans were obtained either immediately before or immediately after the SPECT scans. The time period covered was 6.77 d. The companion time series provides an opportunity to compare complete measured SPECT time–activity curves for individual tumors with the complete measured conjugate-view time–activity curve for the composite tumor.

RESULTS

Tumor Dosimetry

The results of hybrid conjugate-view–SPECT tumor dosimetry for abdominal and pelvic tumors are given in Table 2. The patient number, the number of tumors evaluated, the minimum and maximum tumor volumes, and the minimum and maximum tumor radiation absorbed doses are listed. The mean number of tumors evaluated per patient was 4.2. Different tumors in the same patient can have similar doses, as with patient 56, in whom the 7 tumors ranged from 174 to

TABLE 2
Radiation Absorbed Dose Range and Volume Range for Abdominal and Pelvic Tumors

Patient no.	No. of tumors evaluated	Volume (cm^3)		Radiation dose (cGy)	
		Min	Max	Min	Max
1	5	2.8	320	541	4044
2	2	34	69	112	307
3	11	2.5	118	77	620
5	1	756	756	466	466
7	4	6.8	455	134	711
10	2	4.4	299	108	982
11	1	795	795	1281	1281
13	2	1.6	246	271	2486
14	2	40	54	730	740
15	1	225	225	402	402
16	4	3.3	65	676	1007
24	2	1.5	48	1071	4018
27	5	4.3	118	483	1039
30	2	13	510	282	1019
31	4	4.1	157	415	1713
32	3	64	197	377	419
34	3	7.1	65	420	628
36	10	1.3	51.5	72	952
37	5	8.0	25	281	1041
39	6	2.3	17	532	1094
42	3	5.5	596	362	1449
43	9	3.7	47	244	662
44	4	24	38	359	777
46	9	3.4	70	84	1272
55	5	3.0	33	221	898
56	7	2.0	25.7	174	608
59	8	1.9	88	116	875
60	1	27	27	321	321
67	2	5.1	25	375	487
69	3	12	92	802	1128
71	5	16	42	216	546

608 cGy, or they can have dissimilar doses, as with patient 24, in whom the 2 tumors differed by 29.5 Gy. The mean value for all 131 tumors in 31 patients was 616 cGy, with a SD of the mean ±50 cGy. The largest dose was 40.4 Gy, and the smallest evaluated dose was 73 cGy. The mean volume for the tumors was 59.2 cm^3 with a SD of the mean of ±11.2 cm^3. The largest volume was 795 cm^3 and the smallest volume was 1.27 cm^3. The smaller volumes had larger errors caused by partial-volume effects from the 1-cm-thick CT slices. The summary statistics for the absorbed dose per unit of administered activity are as follows: mean, 1.83 Gy/GBq; and SD, ±0.145 Gy/GBq. The largest value was 12.6 Gy/GBq, and the smallest value was 0.149 Gy/GBq.

A plot of the radiation absorbed dose versus volume for each abdominal and pelvic tumor is presented in Figure 1A. The least-squares fit to the data, the best-fit equation, and the square of the correlation coefficient, r^2, are also presented in the graph. The r^2 value was only 0.007, indicating that very little of the variation in the absorbed dose was caused by a linear dependence on volume. In addition, the slope of the best fit yielded a decrease of only 36.4 cGy in absorbed dose (5.9% of the mean tumor dose) for a 100-cm^3 increase in volume.

Figure 1B presents a plot of $\log_{10}$ (D) versus $\log_{10}$ (V) to show the individual tumor values with less overlap of datapoint symbols. More than half of the tumors (57%) had a $\log_{10}$ (D) value between 2.25 and 3.00 with a $\log_{10}$ (V) value between 0.50 and 2.00. These values correspond to between 178 and 1000 cGy and between 3.2 and 100 cm^3.

The plot of radiation absorbed dose per unit of administered activity versus volume and its least-squares fit looks similar to Figure 1A. The r^2 value (0.010) was only slightly larger than that for the absorbed dose.

The results of hybrid conjugate-view–SPECT tumor dosimetry for the smaller number of axillary tumors are given in Table 3. The mean value for the 9 tumors was 158 cGy, with a SD of ±7.00 cGy. The largest dose was 185 cGy and the smallest dose was 125 cGy. A 2-tailed *t* test revealed that the mean absorbed dose for the axillary tumors is different from that for the abdominal and pelvic tumors in a statistically significant way ($P = 0.01$). The mean volume for the tumors was 69.5 cm^3 with a SD of ±16.0 cm^3. The largest volume was 151 cm^3 and the smallest was 24.1 cm^3. The summary statistics for the absorbed dose per unit of administered activity are as follows: mean, 0.440 Gy/GBq; and SD, ±0.0527 Gy/GBq. The largest value was 0.719 Gy/GBq and the smallest value was 0.270 Gy/GBq.

Tests of Curve–Shape Assumption

Intratherapy SPECT Time Series. Patient 16 had 4 tumors located within the abdomen. At each of the 3 time points, the SPECT %ID was evaluated for each tumor, and then the values were summed. The intraevaluation, conjugate-view results had a single, corresponding composite tumor, which was evaluated over a longer time span. One of the conjugate-view times for evaluation coincided with the earliest SPECT time point. Because interest here is in comparing the washout curve shapes, SPECT %ID results were normalized to the conjugate-view %ID at this earliest SPECT time point and the earlier conjugate-view points neglected. Figure 2 presents the SPECT results for the sum of the 4 individual tumors and the conjugate-view results for the composite tumor. It can be seen that the curves match quite well.

Intraevaluation SPECT Time Series. For patient 43, the plot of the sum over 9 tumors of the %ID from SPECT versus time after infusion and the conjugate-view curve for

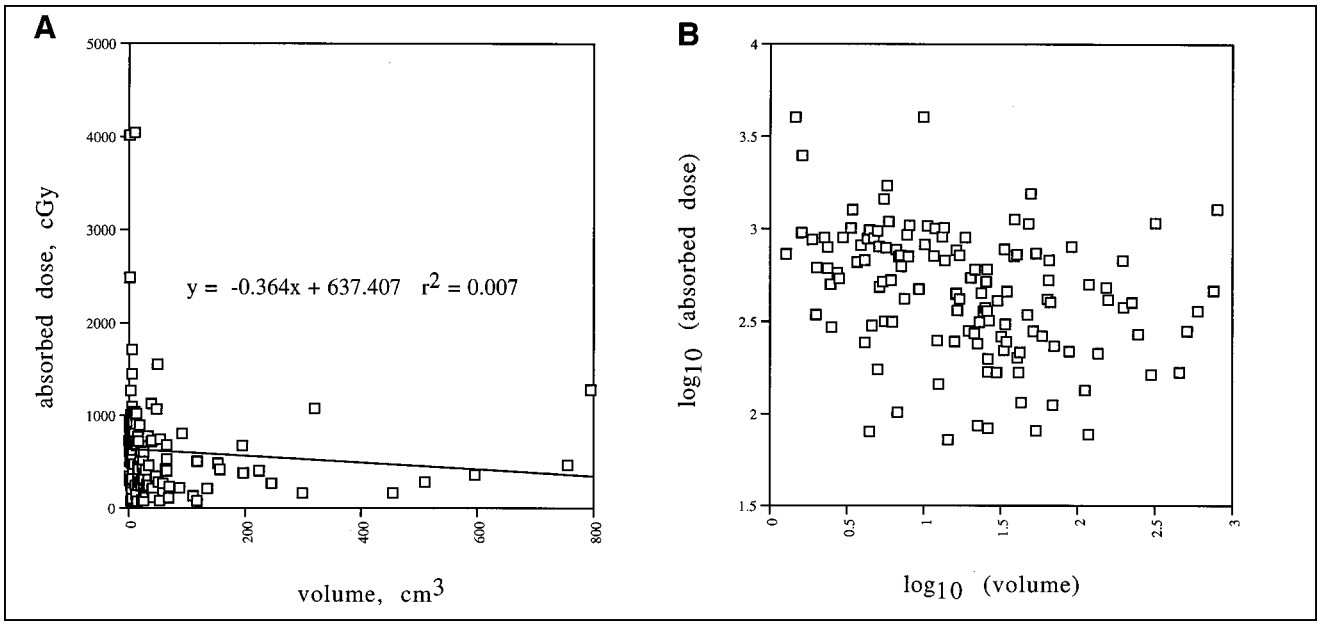

FIGURE 1. Plots of radiation absorbed dose for each tumor versus tumor volume. (A) Linear plot. (B) $\log_{10}$ of absorbed dose versus $\log_{10}$ of volume.

TABLE 3
Radiation Absorbed Dose Range and Volume Range for Axillary Tumors

Patient no.	No. of tumors evaluated	Volume (cm^3)		Radiation dose (cGy)	
		Min	Max	Min	Max
51	1	24	24	149	149
55	2	45	58	141	184
61	2	49	69	125	151
67	2	151	151	171	185
71	2	36	43	144	175

the composite tumor are shown in Figure 3. The largest intraevaluation conjugate-view value has been normalized to the largest SPECT value. The conjugate-view curve is noisier than the SPECT curve, but there is good agreement in the general curve shapes.

The SPECT time series for each of the individual tumors was considerably noisier than that for the sum over 9 tumors. Because of the noise, one could not say whether individual tumors had different curve shapes. However, in addition to the method that uses TEW scatter compensation, which was standard for the 3000 model camera and was used above, a calibration for the method that uses a variable conversion factor without explicit scatter compensation was also available for the camera. A second evaluation of the individual tumors was performed with it. With this second quantification, the shapes appeared to fall into 2 categories, the first being an instantaneous peak and the second category being a peak at 24 h. The 3 tumors in category 1 are shown in Figure 4A, and the 5 tumors that fall into category 2 are plotted in Figure 4B. The 1 tumor with the noisiest curve shape does not fit easily into either category and so is not plotted. Note that the %ID at the earliest time point has been normalized to that of the location right of the aorta, ''rtaor,'' tumor for all cases.

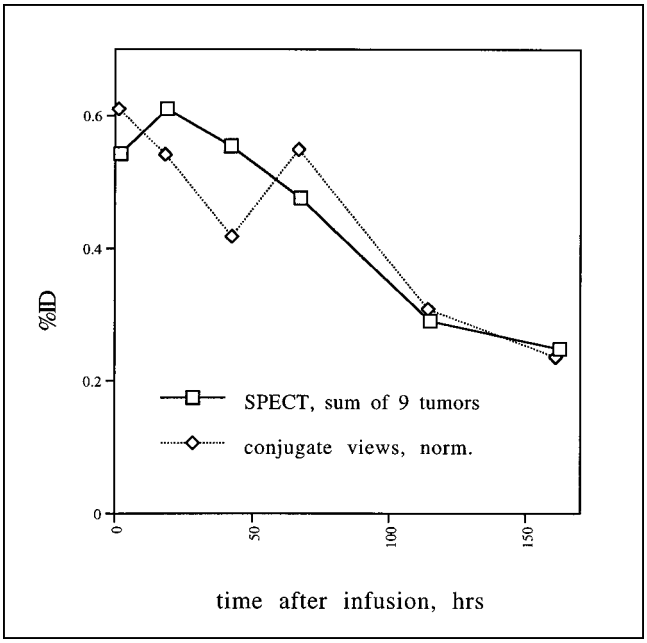

FIGURE 3. Shape comparison for SPECT and conjugate-view intraevaluation time–activity curves for patient 43. Plot of sum over 9 tumors of SPECT activity as %ID versus time after infusion. Conjugate-view values for single, corresponding, composite tumor have been normalized (norm.) so largest conjugate-view value equaled largest SPECT value.

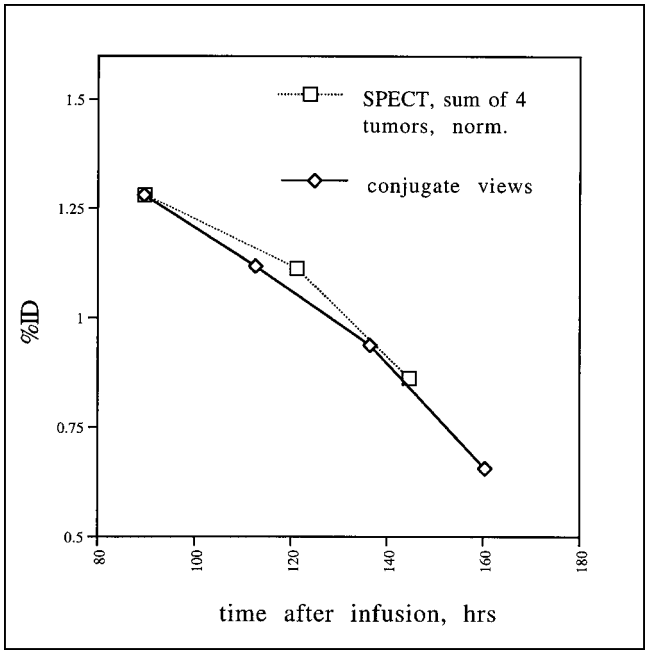

FIGURE 2. Shape comparison for intratherapy SPECT and intraevaluation conjugate-view time–activity curves for patient 16. Plot of activity as percentage of decay-corrected %ID versus time after infusion.

DISCUSSION

Because the mean of the absorbed dose for the group of abdominal and pelvic tumors and that for the group of axillary tumors were different at a statistically significant ($P = 0.01$) level, these 2 groups of tumors should be analyzed separately in assessing dose–response relationships. The mechanism for the increase in radiation dose for the abdominal and pelvic tumors compared with the axillary tumors may possibly be occasional activity spillover from nearby organs and major blood vessels within the main part of the trunk. This spillover would presumably be greater than general background spillover. The latter is being accounted for with a model that uses a uniform distribution.

The correlation coefficient for radiation absorbed dose versus volume for the abdominal and pelvic tumors was small ($r^2 = 0.007$), and the slope of the best-fit line displayed a decrease of only 36.4 cGy in absorbed dose (5.9% of the mean tumor dose) for a 100-g increase in tumor size. These results are in contrast with those from a phase 1/2 RIT trial with the ^{131}I-labeled anticarcinoembryonic antigen

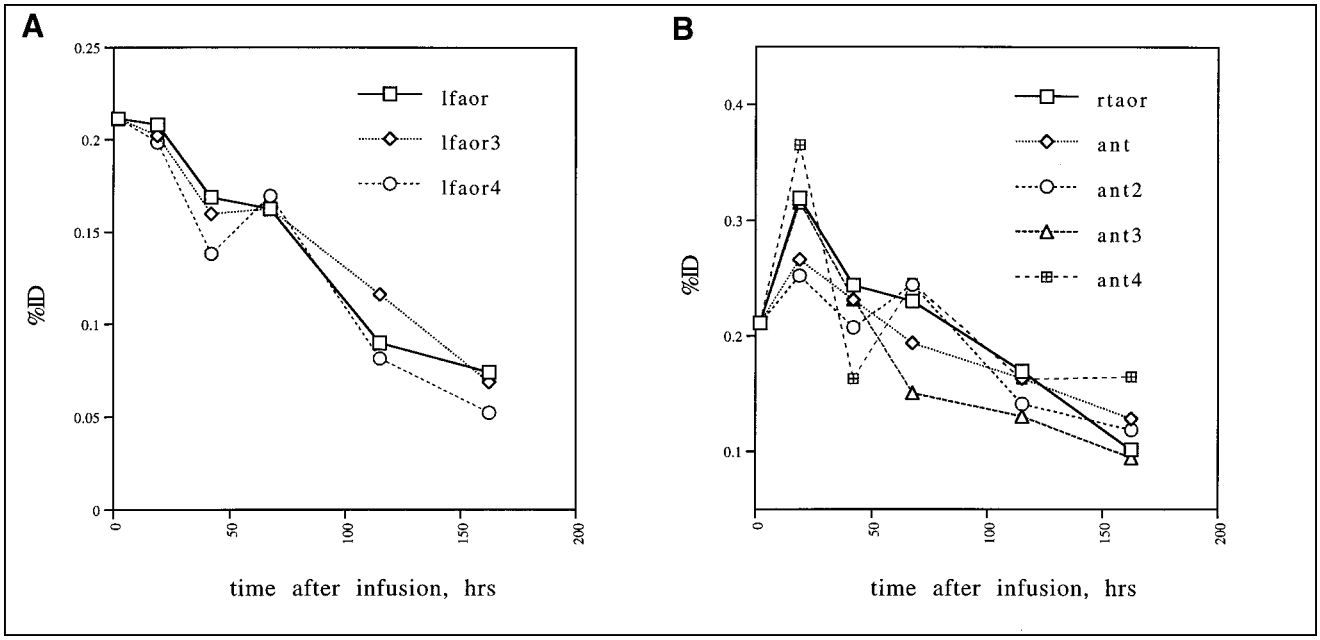

FIGURE 4. Shape comparison for time–activity curves for individual tumors of patient 43. Plot of activity as %ID for 8 of 9 tumors. (A) Three tumors exhibited instantaneous peak uptake. ''Lfaor'' refers to their location being left of the aorta. (B) Five tumors showed peak uptake at 24 h. ''Rtaor'' refers to a location right of the aorta and anterior (ant) to a location more anterior than the aorta tumors. The ninth tumor had noisiest curve and did not fit into either category and, so, was not plotted.

(CEA) murine monoclonal antibody, NP-4, for patients with CEA-expressing tumors from colorectal, lung, pancreatic, breast, or medullary-thyroid cancer (*21*). The authors stated that there is ''. . .a strong dependence of antibody uptake in the CEA-expressing tumor lesions on tumor size,'' and the logarithm of the tumor dose in cGy/mCi plotted against tumor mass has a r^2 value of 0.548. The response rates for this therapy–patient system (*21*) are less than those in anti-B_1 therapy (*6*). Therefore, the small slope in anti-B_1 therapy of previously untreated patients may be a characteristic that is important for relatively good response.

The mean radiation absorbed dose per unit of administered activity for the abdominal and pelvic tumors, 1.83 ± 0.145 Gy/GBq, was slightly higher than the 2 tumor radiation doses previously measured for anti-B_1–antibody therapy of previously treated patients, 1.7 and 1.4 Gy/GBq (*10*). However, the new mean overlaps, within 2 SDs of the mean, the higher of these 2 values and almost overlaps the lower. On the other hand, the mean for anti-B_1–antibody therapy of previously untreated patients is considerably higher than the mean for the ^{131}I-Lym-1 therapy of patients with either non-Hodgkin's lymphoma or chronic lymphocytic leukemia (*22*). The mean tumor dose in that study was 1.0 Gy/GBq with a range of 0.1–3.5 Gy/GBq (*22*). If the unstated SD is the same as for the current anti-B_1–antibody data, then the difference between the means (0.83 Gy/GBq) is 5.7 SDs.

For a given patient, the time–activity curve for the sum of the intratherapy activities from individual SPECT tumors had the same washout shape as the intraevaluation time–activity curve for the composite tumor evaluated by conjugate views. This result tends to justify the use of the intraevaluation conjugate-view time curve as a single, general shape that approximates the intratherapy SPECT time–activity curves of individual SPECT tumors. In a different patient, a similar sum of intraevaluation activities from individual SPECT tumors yielded a time–activity curve that matched the shape of the intraevaluation time–activity curve for the composite tumor evaluated by conjugate views. Therefore, the conjugate-view curve shape was again providing a good approximation to the average SPECT curve shape.

The question of intratherapy time–activity curves being the same for each and every individual SPECT tumor was addressed by other anecdotal data. In 1 patient evaluated, there was evidence that the curve shapes for individual tumors fell into 2 general curve shapes distinguished by different times to peak %ID. This result implies that a single conjugate-view curve shape is not completely accurate for all of the individual tumors. Physiologically, if confirmed by other patients, this result might imply that certain lymphoma tumors are more avid for the circulating anti-B_1 antibody than other tumors in the same patient or that they have a better blood supply.

A preliminary analysis of radiation dose and degree of response has been performed for the abdominal and pelvic tumors of 20 patients (*23*). Using a multiple-measures statistical technique, there was a trend toward a statistically significant correspondence of high radiation dose with a complete response. Because the number of partial responders was small, further analysis is needed.

CONCLUSION

Hybrid SPECT–conjugate-view dosimetry provides radiation absorbed dose estimates for individual lymph node tumors that are defined from CT ROIs. In anti-B_1 therapy of previously untreated non-Hodgkin's lymphoma patients, the radiation dose absorbed by the individual tumors does not correlate strongly with their pretherapy volumes, and, on average, there is only a small decrease in radiation dose with an increase in volume. Axillary tumors have a statistically significant lower radiation dose than that for abdominal or pelvic tumors and should be analyzed separately in dose–response studies.

ACKNOWLEDGMENTS

The authors gratefully acknowledge the assistance of Chuck Meyer in providing the fusion program and Jeff Fessler in making the SAGE reconstruction program available. The technical assistance of Paul Kison, Nancy McCullough, Andrew Paberzs, Sharon Lin, Fahim Razzaque, Sheila Shah, and Virginia Rogers is also appreciated. This work was supported by grants R01 CA38790, CA42768, and CA56794, awarded by the National Cancer Institute, U.S. Department of Health and Human Services; grant M01 RR042, awarded by the National Center for Research Resources, National Institutes of Health, U.S. Department of Health and Human Services; and by a grant from Coulter Pharmaceutical. The contents are solely the responsibility of the authors and do not necessarily represent the official views of the National Cancer Institute.

REFERENCES

1. Press O, Early J, Appelbaum F, et al. Phase II trial of I-131 B1 (anti-CD20) antibody therapy with autologous stem cell transplantation for relapsed B-cell lymphomas. *Lancet*. 1995;346:336–340.
2. Kaminski MS, Zasadny KR, Francis IR, et al. Iodine-131-anti B1 radioimmunotherapy for B-cell lymphoma. *J Clin Oncol*. 1996;14:1974–1981.
3. DeNardo GL, O'Donnell RT, Oldham RK, DeNardo SJ. A revolution in the treatment of non-Hodgkin's lymphoma. *Cancer Biother Radiopharm*. 1998;13:213–223.
4. Wahl RL, Zasadny KR, McFarlane D, et al. Iodine-131 anti-B1 antibody for B-cell lymphoma: An update on the Michigan phase I experience. *J Nucl Med*. 1998;39:21S-27S.
5. Stagg R, Wahl RL, Estes J, et al. Phase I/II study of iodine-131 anti-B1 antibody for non-Hodgkin's lymphoma [abstract]. *Proc Am Soc Clin Oncol*. 1998;17:39a.
6. Kaminski MS, Gribbin T, Estes J, et al. Iodine-131-anti B1 antibody for previously untreated follicular lymphoma (FL): clinical and molecular remissions [abstract]. *Proc Am Soc Clin Oncol*. 1998;17:2a.
7. Wahl RL, Zasadny KR, Estes JM, et al. University of Michigan Cancer Center iodine-131 anti-B_1 antibody clinical experience [abstract]. *J Nucl Med*. 1999; 40:19P.
8. DeNardo GL, DeNardo SJ, Shen S, et al. Pilot studies of radioimmunotherapy of B cell lymphoma and leukemia using 131-I-Lym-1 monoclonal antibody. *Antibody Immunoconj Radiopharm*. 1988;1:17–33.
9. Meredith RF, Johnson TK, Plott G, et al. Dosimetry of solid tumors. *Med Phys*. 1993;20(pt. 2):583–592.
10. Koral KF, Zasadny KR, Kessler ML, et al. CT–SPECT fusion plus conjugate views for determining dosimetry in iodine-131-monoclonal antibody therapy of lymphoma patients. *J Nucl Med*. 1994;35:1714–1720.
11. Koral KF, Li J, Dewaraja Y, et al. I-131 anti-B1 therapy/tracer uptake ratio using a new procedure for fusion of tracer images to CT images. *Clin Cancer Res*. 1998;5:3004s–3009s.
12. Koral KF, Zasadny KR, Swailem FM, et al. Importance of intra-therapy single-photon emission tomographic imaging in calculating tumour dosimetry for a lymphoma patient. *Eur J Nucl Med*. 1991;18:432–435.
13. Koral KF, Zasadny KR, Ackermann RJ, Ficaro EP. Deadtime of two multi-head Anger cameras in ^{131}I dual-energy-window-acquisition mode. *Med Phys*. 1998;25: 85–91.
14. Meyer CR, Boes JL, Kim B, et al. Demonstration of accuracy and clinical versatility of mutual information for automatic multimodality image fusion using affine and thin-plate spline warped geometric deformations. *Med Image Anal*. 1997;1:195–206.
15. Ogawa K, Harata Y, Ichihara T, Kubo A, Hashimoto S. A practical method for position dependent Compton scatter compensation in single photon emission CT. *IEEE Trans Med Imaging*. 1991;10:408–412.
16. Fessler JA, Hero AO. Penalized maximum-likelihood image reconstruction using space-alternating generalized EM algorithms. *IEEE Trans Image Processing*. 1995;4:1417–1429.
17. Koral KF, Dewaraja Y, Lin S. ^{131}I tumor quantification a new background-adaptive method [CD-ROM]. IEEE Nuclear Science Symposium [Conference record], Albuquerque, NM: 1997.
18. Dewaraja Y, Li J, Koral K. Quantitative I-131 SPECT with triple energy window Compton scatter correction. *IEEE Trans Nucl Sci*. 1998;45:3109–3114.
19. Koral KF, Dewaraja Y. I-131 SPECT activity recovery coefficients with implicit or triple-energy-window scatter correction. *Nucl Instrum Methods Phy Res Sect A*. 1999;A 422:688–692.
20. Loevinger R, Budinger TF, Watson EE. MIRD primer for absorbed dose calculations. New York, NY: Society of Nuclear Medicine; 1988.
21. Behr TM, Sharkey RM, Juweid M, et al. Phase I/II clinical radioimmunotherapy with an I-131-labeled anti-carcinoembryonic antigen murine monoclonal antibody IgG. *J Nucl Med*. 1997;38:858–870.
22. DeNardo GL, DeNardo SJ, Shen S, et al. Factors affecting ^{131}I-Lym-1 pharmacokinetics and radiation dosimetry in patients with non-Hodgkin's lymphoma and chronic lymphocytic leukemia. *J Nucl Med*. 1999;40:1317–1326.
23. Koral KF, Dewaraja Y, Clarke LA, et al. Tumor absorbed dose estimates versus response in tositumomab therapy of previously-untreated patients with follicular non-Hodgkin's lymphoma: preliminary report. *Cancer Biother Radiopharm*. 2000;15:August.